Exploring anomalous $HZ\gamma$ couplings in γ-proton collisions at the LHC

S. Taheri Monfared, Sh. Fayazbakhsh and M. Mohammadi Najafabadi

School of Particles & Accelerators,
Institute for Research in Fundamental Sciences (IPM)

Institute for Research in Fundamental Sciences

DIS 2016
(11 - 15 April 2016)
DESY Hamburg, Germany

Outline

1. Introduction
   - The Feynman diagrams
2. The effective lagrangian and anomalous interactions
   - The effective lagrangian
   - The anomalous interactions
3. The numerical analysis of Higgs production cross section
   - EPA
   - PDF
   - Total cross section
4. 95% C.L. limits on the anomalous couplings
   - Results on $\sqrt{s} = 14$ TeV
   - Results on $\sqrt{s} = 100$ TeV
   - The contour diagrams
5. Conclusion

Outline

Motivation

- ✓ The SM predictions are currently approved to elucidate several experimental phenomena in particle physics. However, there is a variety of physical points which cannot be explained by this effective theory and this is a sensible reason to go BSM.
- ✓ Although there has not been observed any direct evidence of NP at the LHC run-I, it is anticipated to discover signals of NP at the LHC run-II.
- ✓ Here an effective Lagrangian is formed from NP inteactions between the elementary particles. Integrating out heavy degrees of freedom at the BSM scale, Λ, some residual interaction terms are obtained including the gauge invariant non-renormalizable effective operators.

In the SM, $HZ\gamma$ boson couple indirectly via loop diagrams, containing massive charged particles. The CMS and ATLAS collaborations have reported that the observed 95% C.L. decay width for the process $H \to Z\gamma$ is 10 and 11 times more than the SM expectation value.

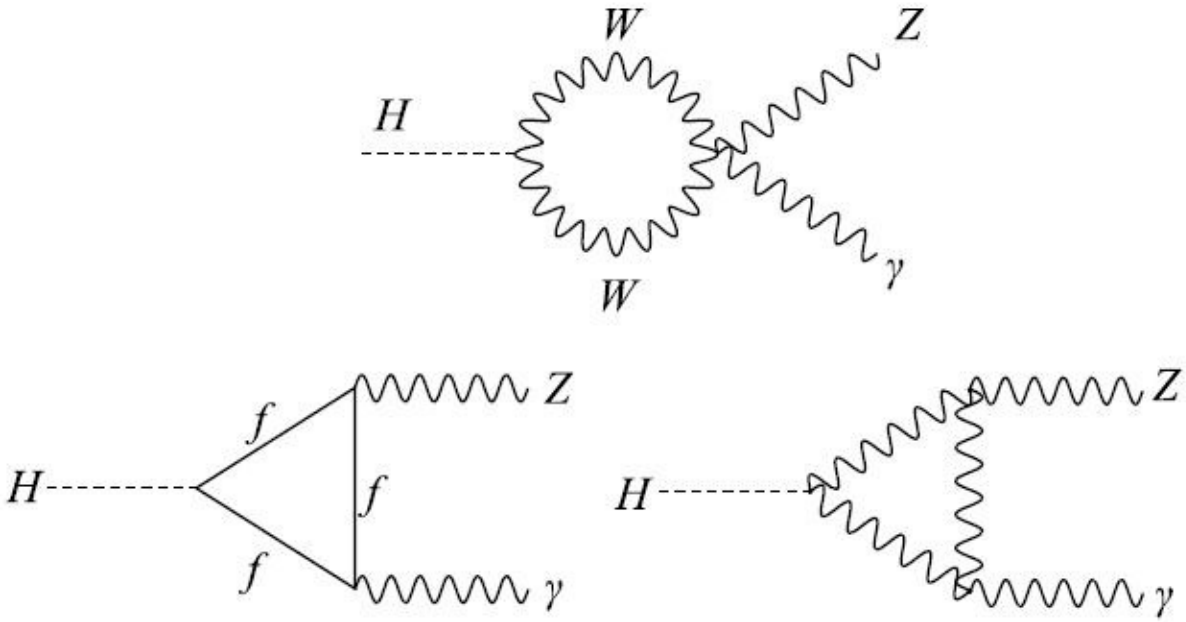

Figure 1: The SM diagrams for $H \to Z\gamma$.

- ✓ The $HZ\gamma$ coupling allows one to consider different kinds of NP hypotheses. Some authors suggest that different particles may circulate in the loop diagrams and the Higgs boson is described as a non-SM scalar field or a massive composite state.
- ✓ The existence of large amounts of CP-violating interactions in NP is highly intriguing.
- ✓ Another motivating aspect is that CP-even and CP-odd structures of anomalous $HZ\gamma$ couplings are both initiated from higher-dimension NP operators.

- ✓ We concentrate on extracting sensitivities of the H production cross section to the anomalous $HZ\gamma$ vertex in single diffractive interactions. Here, one of the protons in a pp collision dissociates while the other one remains intact and scatters at small angles. It loses a fractional proton energy, ξ, and this parameter specifies the detector acceptance region in which forward intact protons are observed.
- ✓ At the LHC energy scale, to a good approximation, $\xi = E_\gamma / E_p$.Three different classes of the acceptance region are considered as
  - $0.0015 < \xi < 0.5$,
  - $0.0015 < \xi < 0.15$,
  - $0.1 < \xi < 0.5$.

The $HZ\gamma$ coupling is studied through the process $pp \to p\gamma p \to pHX$ at the LHC using the effective Lagrangian approach. Both the CP-conserving and -violating interactions arising from dimension six operators are considered.

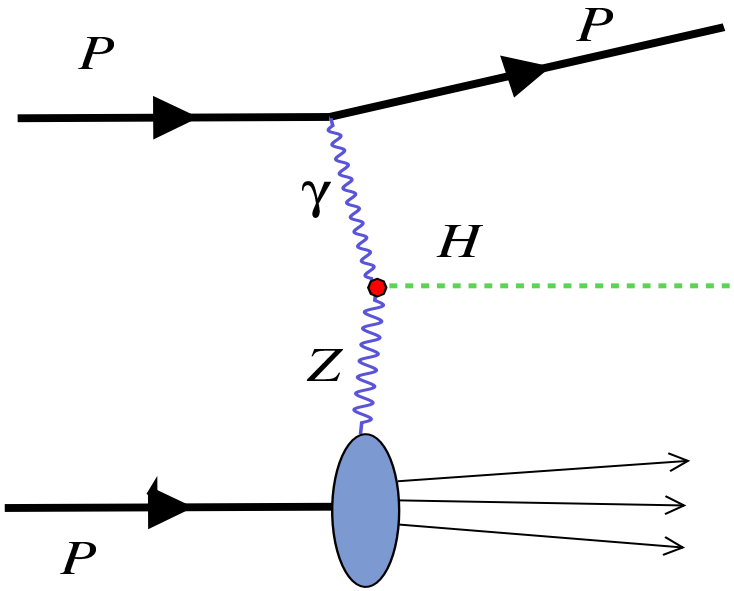

Figure 2: A schematic Feynman diagram of the process $pp \to pHX$.

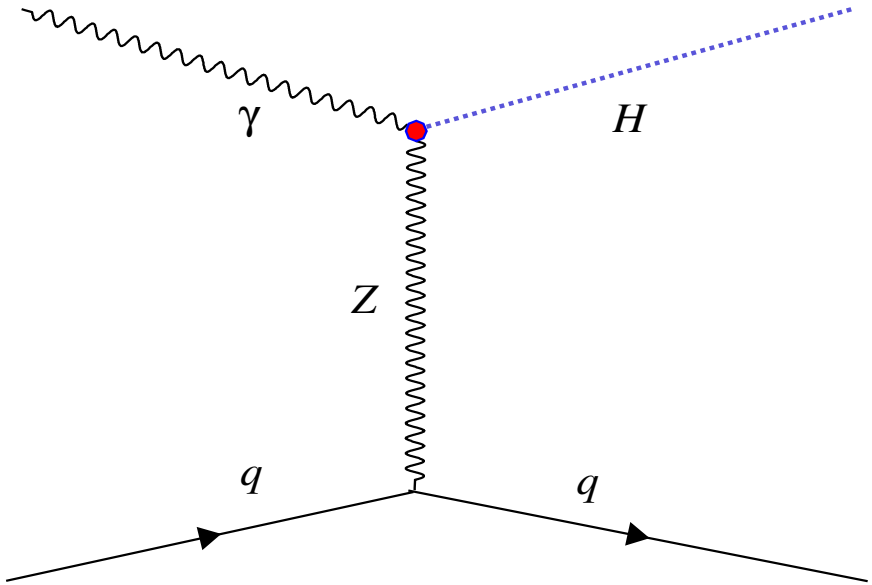

Figure 3: A representative leading-order Feynman diagram of the subprocess $\gamma q \to \gamma Z q \to Hq$.

Outline

The effective lagrangian and anomalous interactions

The SM predictions for the $HZ\gamma$ coupling is based on the heavy quarks and W boson loops computations.
We start with an effective Lagrangian involving the effects of non-SM fields interactions. This Lagrangian can be obtained by the generalization of the SM interaction terms, from all dimension four operators to higher-dimension ones. The expansion of the effective Lagrangian at dimension six operators:

$$\mathcal{L}_{\text{eff.}} = \mathcal{L}_{\text{SM}} + \sum_i \frac{c_i^{(6)} \mathcal{O}_i^{(6)}}{\Lambda^2} + H.c., \tag{1}$$

- $c_i^{(6)} \rightarrow$ Dimensionless Wilson coefficients
- $\mathcal{O}_i^{(6)} \rightarrow$ Gauge invariant local operators

After the EWSB, the effective Lagrangian in the Higgs sector with $HZ\gamma$ vertex is described in terms of the physical fields interactions as

$$\mathcal{L}^{(6)}_{\text{eff.}} = g^{(1)}_{HZ\gamma}\partial_\nu H Z_\mu A^{\mu\nu} + g^{(2)}_{HZ\gamma} H A_{\mu\nu} Z^{\mu\nu} + \tilde{g}_{HZ\gamma} H \tilde{Z}_{\mu\nu} A^{\mu\nu} + H.c.. \quad (2)$$

- $B_{\mu\nu}$ are the field strength tensors for $B \equiv A, Z$ gauge bosons and $\tilde{B}_{\mu\nu} = \frac{1}{2}\varepsilon_{\mu\nu\rho\sigma}B^{\rho\sigma}$, $\varepsilon^{0123} = 1$.
- $g^{(1,2)}_{HZ\gamma} \rightarrow$ The coefficients of the CP-even operators.
  $\tilde{g}_{HZ\gamma} \rightarrow$ The coupling regarding the CP-odd interaction term.
- In a compact form: $\mathcal{L}^{(6)}_{\text{eff.}} = HZ_\mu T^{\mu\nu} A_\nu + H.c.$,
  $T^{\mu\nu}(q,k) = \hat{\alpha}k^2 g^{\mu\nu} + \alpha_1(q,k)\,[k\cdot q g^{\mu\nu} - k^\mu q^\nu] + \alpha_2(q,k)\,\varepsilon^{\mu\nu\rho\sigma}k_\rho q_\sigma.$
- By plugging the above vertex into Eq. (2),
  $$\hat{\alpha} \equiv -g^{(1)}_{HZ\gamma}$$
  $$\alpha_1 \equiv -g^{(1)}_{HZ\gamma} + 2g^{(2)}_{HZ\gamma}$$
  $$\alpha_2 \equiv 2\tilde{g}_{HZ\gamma}$$
- At leading order results of the SM: $\hat{\alpha}^{\text{SM}} = \alpha_1^{\text{SM}} = \alpha_2^{\text{SM}} = 0$.

Outline

The total scattering amplitude $\overline{|M|}^2$ with

- the redefinition of vector and axial-vector couplings, $C_{\mathsf{q}}^{\pm} = C_{\mathsf{q,V}}^2 \pm C_{\mathsf{q,A}}^2$
- using the relation $\hat{s} + \hat{t} + \hat{u} = m_{\mathsf{H}}^2 + 2m_{\mathsf{q}}^2$

is $\overline{|M|}^2 = \overline{|M_1|}^2 \alpha_1^2(q,k) + \overline{|M_2|}^2 \alpha_2^2(q,k)$

$$\overline{|M_1|}^2 = -\frac{g_{\mathsf{Z}}^2}{8(m_{\mathsf{Z}}^2 - \hat{t})^2}\left\{C_{\mathsf{q}}^{+}\hat{t}\left((\hat{t}+\hat{s}-m_{\mathsf{q}}^2-m_{\mathsf{H}}^2)^2 + (\hat{s}-m_{\mathsf{q}}^2)^2\right) + 2C_{\mathsf{q}}^{-}\, m_{\mathsf{q}}^2(m_{\mathsf{H}}^2-\hat{t})^2\right\},$$

$$\overline{|M_2|}^2 = -\frac{g_{\mathsf{Z}}^2}{4(m_{\mathsf{Z}}^2 - \hat{t})^2}(m_{\mathsf{H}}^2-\hat{t})^2\left\{C_{\mathsf{q}}^{+}(\hat{t}-2m_{\mathsf{q}}^2) + 4C_{\mathsf{q}}^{-}\, m_{\mathsf{q}}^2\right\}. \tag{4}$$

A technical tool to perform the numerical calculations of a γ-induced subprocess, is the EPA method. This is applied to the forward direction collisions ($Q^2/E_\gamma^2 \ll 1$). The emitted photon is considered as a quasireal particle whose spectrum with respect to its energy and virtuality is given by

$$f(E_\gamma, Q^2) = \frac{dN}{dE_\gamma dQ^2} = \frac{\alpha_e}{\pi}\frac{1}{E_\gamma Q^2}\left[(1-\frac{E_\gamma}{E_p})(1-\frac{Q^2_{min}}{Q^2})F_E + \frac{E_\gamma^2}{2E_p^2}F_M\right], \quad (5)$$

$$F_E = \frac{4m_p^2 G_E^2 + Q^2 G_M^2}{4m_p^2 + Q^2}, \quad F_M = G_M^2, \quad Q^2_{min} = \frac{E_\gamma^2 m_p^2}{E_p(E_p - E_\gamma)},$$
$$G_E^2 = \frac{G_M^2}{\mu_p^2} = (1+\frac{Q^2}{Q_0^2})^{-4}, \quad Q_0^2 = 0.71\ GeV^2, \quad \mu_p^2 = 7.78. \quad (6)$$

- The F_E and F_M functions are determined by the proton electric and magnetic form factors, respectively.
- $E_\gamma = E_p\xi$ in the EPA.

To generate hard scattering matrix elements, we take the results of three main PDF fitting collaborations,

- CTEQ14
- NNPDF3.0
- MMHT14

The uncertainty due to the choice of a particular PDF set arises from limited knowledge of the proton structure. It is estimated by performing all computations of the signal cross sections for different PDF sets. We have the PDF uncertainties of

(I) $0.022\% \rightarrow$ for the first acceptance region

(II) $0.019\% \rightarrow$ for the second acceptance region

(III) $0.161\% \rightarrow$ for the third acceptance region

The total cross section is derived by convoluting the subprocess cross section with the EPA method and the aforementioned PDF sets:

$$\sigma = \sum_{q=u,d,s,c,b} \int_{\omega_{\min}}^{\omega_{\max}} \frac{\omega}{2E_p y} d\omega \int_{y_{min}}^{y_{max}} dy \int_{Q^2_{1,min}}^{Q^2_{1,max}} dQ_1^2 \; f_\gamma(y, Q_1^2),$$
$$f_q\left(\frac{\omega^2}{4E_p y}, Q_2^2\right) \; \hat{\sigma}_{Z\gamma \to H}(Q_1^2, \omega, y) \tag{7}$$

with the integration limits of

$$y_{\min} = \text{Max}\left[\frac{\omega^2}{4E_p x_{\max}}, E_p \xi_{\min}\right], \;\; y_{\max} = \text{Min}\left[\frac{\omega^2}{4E_p x_{\min}}, E_p \xi_{\max}\right],$$
$$\omega_{\min} = \text{Max}\left[2E_p\sqrt{\xi_{\min} x_{\min}}, m_H + m_q\right], \;\; \omega_{\max} = 2E_p\sqrt{\xi_{\max} x_{\max}}, \tag{8}$$

- $Q_2 = \mu_f = \mu_r = m_H$ (the threshold production scale)
- Deviations due to the variation of scales are found to be
  - (I) $0.004\% \rightarrow$ for the first acceptance region
  - (II) $0.012\% \rightarrow$ for the second acceptance region
  - (III) $0.054\% \rightarrow$ for the third acceptance region
- The third region results contain the largest uncertainty coming from the factorization scale variations and the choice of PDF.
- Both kind of uncertainties increase with increasing center of mass energy from $\sqrt{s} = 14$ TeV to $\sqrt{s} = 100$ TeV.
- The uncertainty due to the choice of PDF is larger than the uncertainty arising from the variation of factorization scale.

The $pp \to pHX$ cross section

No considerable difference exists between α_1 and α_2.

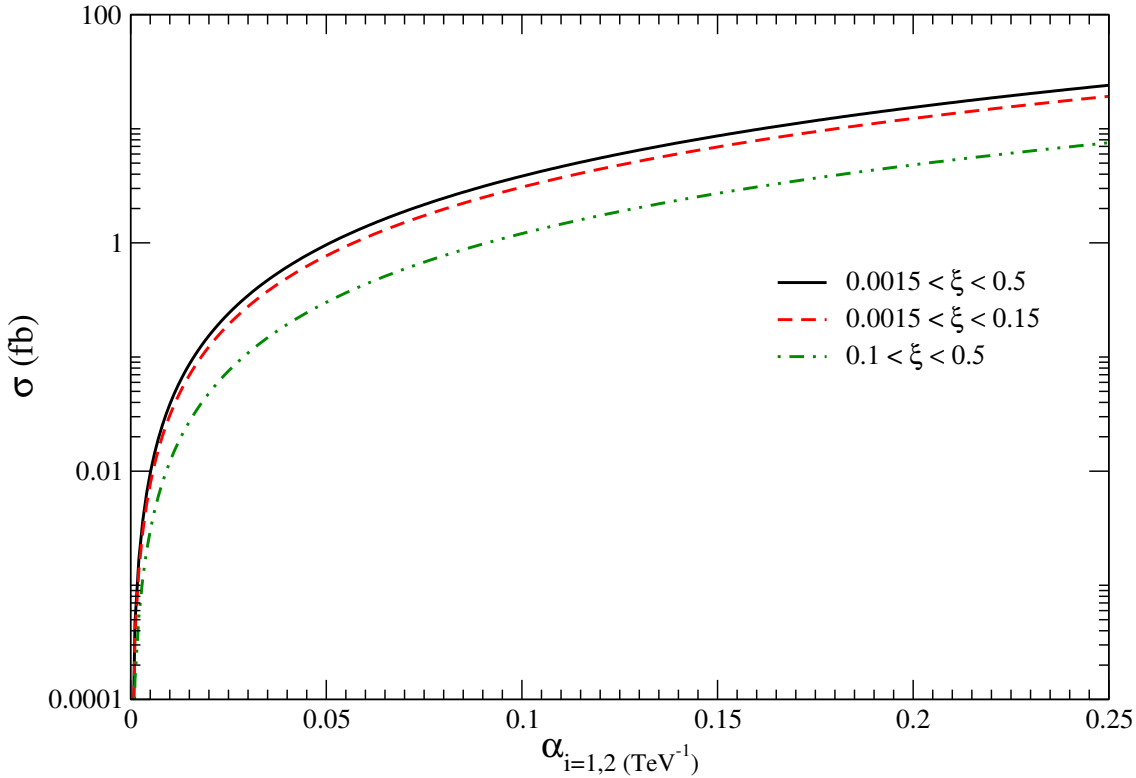

Figure 4: The total cross section of the process $pp \to pHX$ as a function of the anomalous coupling $\alpha_{1(2)}$ at $\alpha_{2(1)} = 0$, at the center of mass energy $\sqrt{s} = 14$ TeV. The curves show the sensitivity for three different acceptance regions remarked on the figure.

Outline

95% C.L. limits on the anomalous couplings at $\sqrt{s} = 14$ TeV

ξ	$\mathcal{L}_{\text{int}}(\text{fb}^{-1})$	$\lvert\alpha_1\rvert = \lvert\alpha_2\rvert$ (TeV^{-1})			
		$H \to \gamma\gamma$	$H \to ZZ$	$H \to W^+W^-$	Combined
First region: $[0.0015 - 0.5]$	100	1.031	0.723	1.390	0.946
	300	0.783	0.550	1.056	0.719
	3000	0.440	0.309	0.594	0.404
Second region: $[0.0015 - 0.15]$	100	1.174	0.788	1.502	1.030
	300	0.892	0.599	1.142	0.782
	3000	0.502	0.337	0.642	0.440
Third region: $[0.1 - 0.5]$	100	0.851	0.861	2.343	1.541
	300	0.647	0.654	1.780	1.171
	3000	0.364	0.368	1.001	0.658

Table 1: Sensitivity of the main process $pp \to pHX$ to the anomalous $HZ\gamma$ couplings, $|\alpha_1|$ and $|\alpha_2|$, at $\sqrt{s} = 14$ TeV and integrated luminosities $\mathcal{L}_{\text{int}} = 100, 300, 3000$ fb^{-1}. The constraints are presented for three different Higgs decay channels, $H \to \gamma\gamma$, $H \to W^+W^-$, and $H \to ZZ$, as well as a combined one achievable with 95% C.L. and for three intervals of forward detector acceptance region, ξ. The CP-even and CP-odd contributions have the same values.

95% C.L. limits on the anomalous couplings at $\sqrt{s} = 100$ TeV

ξ	$\mathcal{L}_{\text{int}}(\text{fb}^{-1})$	$\lvert\alpha_1\rvert = \lvert\alpha_2\rvert$ (TeV^{-1})			
		$H \to \gamma\gamma$	$H \to ZZ$	$H \to W^+W^-$	Combined
First region: $[0.0015 - 0.5]$	100	0.278	0.255	0.619	0.408
	300	0.210	0.194	0.470	0.310
	3000	0.118	0.109	0.264	0.174
Second region: $[0.0015 - 0.15]$	100	0.297	0.267	0.629	0.416
	300	0.226	0.203	0.478	0.316
	3000	0.127	0.114	0.269	0.178
Third region: $[0.1 - 0.5]$	100	0.051	0.221	0.919	0.602
	300	0.039	0.168	0.699	0.458
	3000	0.022	0.095	0.393	0.257

Table 2: Sensitivity of the main process $pp \to pHX$ to the anomalous couplings of the $HZ\gamma$ vertex at $\sqrt{s} = 100$ TeV. See the caption of table 1 for further details.

The contour diagrams in $\alpha_1 - \alpha_2$ plane

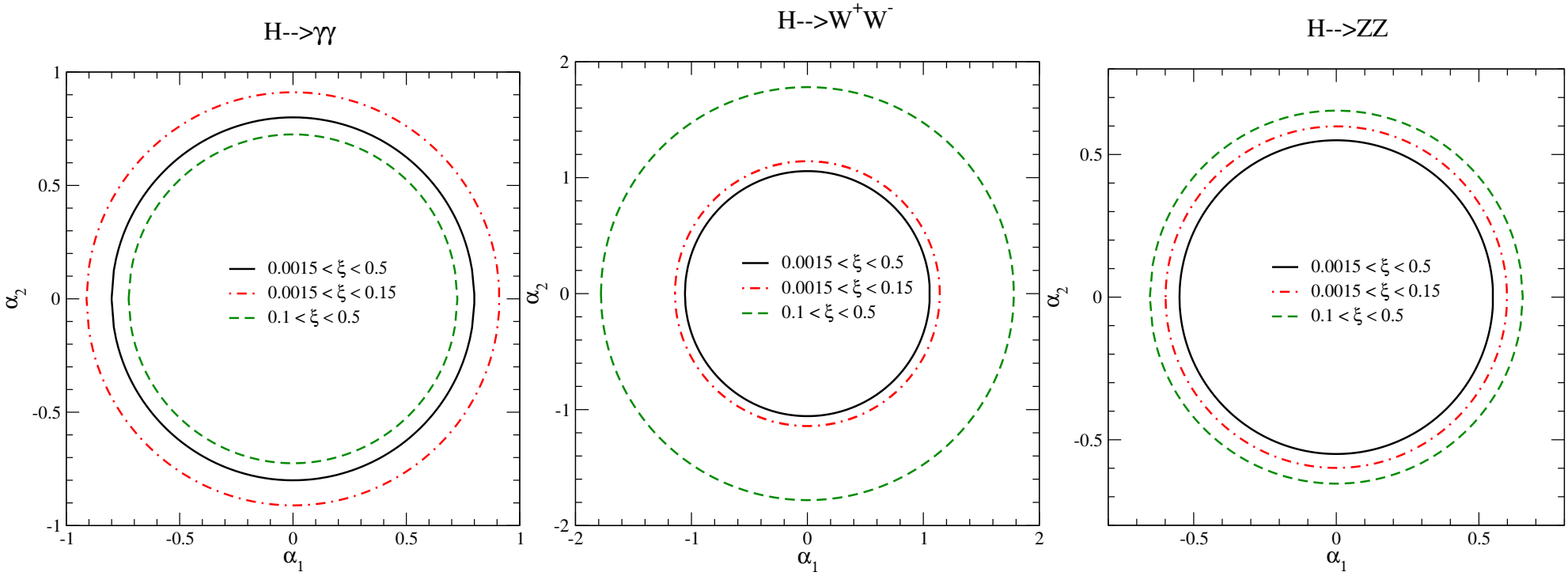

Figure 5: The contour diagrams in $\alpha_1 - \alpha_2$ plane for three different Higgs decay channels of $H \to \gamma\gamma$, $H \to W^+W^-$, and $H \to ZZ$ with $95\%\ C.L.$ at $\sqrt{s} = 14$ TeV and $\mathcal{L}_{\text{int}} = 300\ \text{fb}^{-1}$. The diagrams are plotted for three different acceptance regions.

Outline

- The present analysis of the process $pp \to pHX$ could be potentiality considered as a first assessment of the LHC to study the $HZ\gamma$ couplings.
- We study the deviations of both CP-even and CP-odd anomalous $HZ\gamma$ couplings from the SM predictions, which arise from NP effects.
- The studied process $pp \to pHX$ shows similar sensitivity to the CP-even and CP-odd couplings.
- The first and second acceptance regions, i.e., $0.0015 < \xi < 0.5$ and $0.0015 < \xi < 0.15$, provide the most restricted bounds in combined channel.
- The best limits on $HZ\gamma$ couplings are obtained from $H \to ZZ$ channel.

We conclude that the process $pp \to pHX$ has a reasonable sensitivity to the anomalous $HZ\gamma$ couplings which complements the results of other channels in search for any deviation of $HZ\gamma$ vertices from the SM predictions.

Thanks for your paying attention

Back-up

To have a more realistic study, we consider

- the irreducible photoproduction background ($\gamma + q \to H + q$) coming from diffractive processes
- as well as the contribution arising from the reducible photoproduction processes. We found that the reducible photoproduction processes, with different particles in the final state, are expected to be effectively rejected by applying the cuts ($p_T^{\gamma,jet,l} \geq 20$ GeV, $|\eta^{\gamma,jet,l}| < 2.5$).

The contribution of the irreducible background is larger than the reducible one after the cuts. The total cross sections of the backgrounds, calculated with CompHEP v4.5.2 package, are summarized in Table 3. We perform an explicit calculation of the background subprocesses when one proton is intact and we have $\gamma\gamma + jet$ (for $H \to \gamma\gamma$ channel), $l_1^{\pm} l_2^{\mp} \nu_{l_1} \nu_{l_2} + jets$ (for $H \to W^+W^-$ channel), and $l_1^{\pm} l_1^{\mp} l_2^{\pm} l_2^{\mp}$ (for $H \to ZZ$ channel) in the final state.

	$\sqrt{s} = 14$ TeV			$\sqrt{s} = 100$ TeV		
Channel	$\gamma\gamma$	ZZ	W^+W^-	$\gamma\gamma$	ZZ	W^+W^-
First region:$[0.0015 - 0.5]$	2.5	0.5	14.4	3.4	2.1	148
Second region:$[0.0015 - 0.15]$	2.7	0.45	12.6	3.6	2	126
Third region:$[0.1 - 0.5]$	0.1	0.09	10	1.3×10^{-4}	0.04	24

Table 3: The total cross sections (unit in fb) of the backgrounds coming from diffractive processes for three final states $\gamma\gamma$, W^+W^-, and ZZ after applying all cuts.

Applying the same cuts on the signal events results in the acceptance efficiencies 0.4, 0.1, and 0.25 for $H \to \gamma\gamma$, $H \to W^+W^-$, and $H \to ZZ$ channels, respectively.

The 95% C.L. constraints

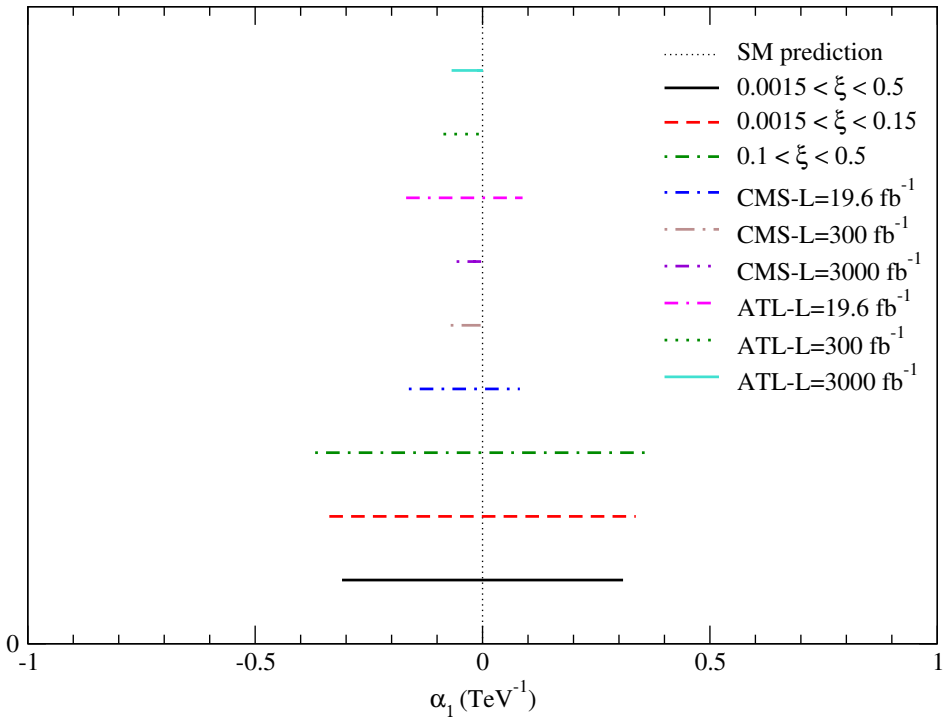

Figure 6: The 95% C.L. constraints for the most conservative combined results based on the dimension six operator coefficients for the LHC at $\sqrt{s} = 14$ TeV with an integrated luminosity of $\mathcal{L}_{\text{int}} = 300$ fb^{-1} for three different acceptance regions. The CMS and ATLAS exclusion limits obtained from the Higgs boson rare decay process are shown for comparison. For completeness, the CMS and ATLAS projected allowed regions are also presented.

The 95% C.L. constraints

By taking into account the most relevant backgrounds (the reducible part) as well as the irreducible ones, and looking at the clean decay modes, i.e., $\gamma\gamma$, W^+W^-, and ZZ, realistic results are obtained.

- Reduction strategies for background processes
- A realistic analysis with using shape variables
- Deriving the background contributions from data

would provide more robust results on the exclusion limits of the anomalous couplings.